Title

Renal ablation using magnetic resonance-guided high intensity focused ultrasound: Magnetic resonance imaging and histopathology assessment

Journal

World Journal of Radiology, 8(3)

ISSN

1949-8470

Authors

Saeed, Maythem
Krug, Roland
Do, Loi
et al.

Publication Date

2016

DOI

10.4329/wjr.v8.i3.298

Peer reviewed

World Journal of Radiology

Submit a Manuscript: http://www.wjgnet.com/esps/
Help Desk: http://www.wjgnet.com/esps/helpdesk.aspx
DOI: 10.4329/wjr.v8.i3.298

World J Radiol 2016 March 28; 8(3): 298-307
ISSN 1949-8470 (online)

ORIGINAL ARTICLE

Basic Study

Renal ablation using magnetic resonance-guided high intensity focused ultrasound: Magnetic resonance imaging and histopathology assessment

Maythem Saeed, Roland Krug, Loi Do, Steven W Hetts, Mark W Wilson

Maythem Saeed, Roland Krug, Loi Do, Steven W Hetts, Mark W Wilson, Department of Radiology and Biomedical Imaging, School of Medicine, University of California San Francisco, San Francisco, CA 94107-5705, United States

Author contributions: Saeed M designed the study, performed the experiments, analyzed MR images/histology and wrote the manuscript; Krug R performed the ablation and MR imaging and involved in manuscript editing; Do L achieved and analyzed the images, prepared the figures and involved in manuscript editing; Hetts SW and Wilson MW provided vital advices and were also involved in manuscript editing.

Institutional review board statement: Departmental Scientific Merit Approval.

Institutional animal care and use committee statement: This study received approval from Institutional Animal Care and Use Committee.

Conflict-of-interest statement: All investigators have no conflict-of-interest.

Data sharing statement: The authors are solely responsible for the data.

Correspondence to: Maythem Saeed, PhD, Professor, Department of Radiology and Biomedical Imaging, School of Medicine, University of California San Francisco, 185 Berry Street, Suite 350, Campus Box 0946, San Francisco, CA 94107-5705, United States. msaeed@ucsf.edu
Telephone: +1-415-5146221
Fax: +1-415-3539423

Received: June 26, 2015
Peer-review started: July 7, 2015
First decision: September 11, 2015
Revised: October 23, 2015
Accepted: November 13, 2015
Article in press: November 17, 2015
Published online: March 28, 2016

Abstract

AIM: To use magnetic resonance-guided high intensity focused ultrasound (MRg-HIFU), magnetic resonance imaging (MRI) and histopathology for noninvasively ablating, quantifying and characterizing ablated renal tissue.

METHODS: Six anesthetized/mechanically-ventilated pigs underwent single/double renal sonication (n = 24) using a 3T-MRg-HIFU (1.1 MHz frequency and 3000J-4400J energies). T2-weighted fast spin echo (T2-W), perfusion saturation recovery gradient echo and contrast enhanced (CE) T1-weighted (T1-W) sequences were used for treatment planning, temperature monitoring, lesion visualization, characterization and quantification, respectively. Histopathology was conducted in excised kidneys to quantify and characterize cellular and vascular changes. Paired Student's t-test was used and a P-value < 0.05 was considered statistically significant.

RESULTS: Ablated renal parenchyma could not be differentiated from normal parenchyma on T2-W or non-CE T1-W sequences. Ablated renal lesions were visible as hypoenhanced regions on perfusion and CE T1-W MRI sequences, suggesting perfusion deficits and necrosis. Volumes of ablated parenchyma on CE T1-W images *in*

vivo (0.12-0.36 cm^3 for single sonication 3000J, 0.50-0.84 cm^3, for double 3000J, 0.75-0.78 cm^3 for single 4400J and 0.12-2.65 cm^3 for double 4400J) and at postmortem (0.23-0.52 cm^3, 0.25-0.82 cm^3, 0.45-0.68 cm^3 and 0.29-1.80 cm^3, respectively) were comparable. The ablated volumes on 3000J and 4400J double sonication were significantly larger than single ($P < 0.01$), thus, the volume and depth of ablated tissue depends on the applied energy and number of sonication. Macroscopic and microscopic examinations confirmed the locations and presence of coagulation necrosis, vascular damage and interstitial hemorrhage, respectively.

CONCLUSION: Contrast enhanced MRI provides assessment of MRg-HIFU renal ablation. Histopathology demonstrated coagulation necrosis, vascular damage and confirmed the volume of damage seen on MRI.

Key words: Magnetic resonance-guided high intensity focused ultrasound; Renal ablation; Magnetic resonance imaging; Microscopy; High intensity focused ultrasound

Core tip: Renal carcinoma constitutes the majority of kidney malignancies. The gold standard procedure for treatment of renal carcinoma remains surgical excision. However, in a large number of patients, surgical excision is precluded by increased perioperative risk due to medical comorbidities. Recent innovations in the field of thermal ablation procedures and real-time imaging have accelerated the development of magnetic resonance-guided high intensity focused ultrasound (MRg-HIFU). This study showed that contrast enhanced magnetic resonance imaging (MRI) provides good assessment of renal ablation created noninvasively by MRg-HIFU. The volume and depth of ablated tissue depends on the applied energy and number of sonications. Histopathology demonstrated coagulation necrosis and vascular damage in the ablated tissue and confirmed the volume of damage seen on contrast enhanced MRI.

Saeed M, Krug R, Do L, Hetts SW, Wilson MW. Renal ablation using magnetic resonance-guided high intensity focused ultrasound: Magnetic resonance imaging and histopathology assessment. *World J Radiol* 2016; 8(3): 298-307 Available from: URL: http://www.wjgnet.com/1949-8470/full/v8/i3/298.htm DOI: http://dx.doi.org/10.4329/wjr.v8.i3.298

INTRODUCTION

The number of renal cell carcinoma cases increases with approximately 65000 new cases diagnosed each year in the United States[1]. The increased use of high-resolution diagnostic imaging has led to the serendipitous detection of small renal tumors in asymptomatic patients with small masses of renal carcinoma[2,3]. The gold standard procedure for treatment of localized renal carcinoma remains surgical excision. However, in a large number of patients, surgical excision is precluded by increased perioperative risk due to medical comorbidities[4,5]. In early 1990, radiofrequency ablation has emerged as a treatment option for this population, with the aim of achieving local oncologic control in a nephron-sparing manner while avoiding the potential morbidity associated with surgical extirpation and general anesthesia. Ritchie *et al*[6] showed that magnetic resonance-guided high intensity focused ultrasound (MRg-HIFU) was effective in two-third of the renal cell carcinoma cases. They suggested that advancement in ablation speed, respiratory navigation and treatment monitoring will improve outcomes and accurate histological analyses are essential in determining treatment efficacy. Innovations in the field of thermal ablation procedures and imaging in the last decade have accelerated the development of MRg-HIFU[7].

There are great differences in heat sensitivity between different cell types and tissues. In order to exploit the use of hyperthermia in the clinic, investigators need a better understanding of heating effects on various cell types and tissues[8]. MRg-HIFU has been used for treating uterine fibroids[9,10], palliation of bone metastases[11], ablation in the brain tumor through the skull[12], breast cancer[13,14], prostate[15] and hepatocellular carcinoma[16]. The safety and feasibility of using extracorporeal HIFU in treating patients with kidney tumor has been demonstrated[17,18]. The objective of this study was to use magnetic resonance imaging (MRI) and histopathology for assessing non-tumor renal ablation in swine model created by MRg-HIFU.

MATERIALS AND METHODS

Animal model

This investigation conformed to National Institutes of Health guidelines for the care and use of laboratory animals and was approved by the Institutional Animal Care and Use Committee. Six farm pigs (mean weight 31.0 ± 1.7 kg) (Pork Power Farms, Turlock, CA) were premedicated with 0.5 mg/kg acepromazine (Fort Dodge Animal Health, Fort Dodge, IA) and 25 mg/kg ketamine (Fort Dodge Animal Health). Animals were anesthetized with a mixture of isoflurane 2%-5% (Abbot Lab., North Chicago, IL) and oxygen and mechanically ventilated. Saline (10 mL/kg per hour) (Abbot Lab., North Chicago, IL) was IV infused. Heart rate, O2-saturation and core body temperature were monitored. Rocuronium bromide (Hospira Inc, Lake Forest, IL) was IV administered prior to ablation to minimize twitching and diaphragm motion during ablation.

MRg-HIFU setting

An MRg-HIFU system (ExAblate 2000, Insightec Ltd, Tirat Carmel, Israel) with a phased array transducer of 208 elements embedded in an MR table was used to create renal ablations. The table was connected to a 3T wide-bore MRI scanner (Discovery MR750w,

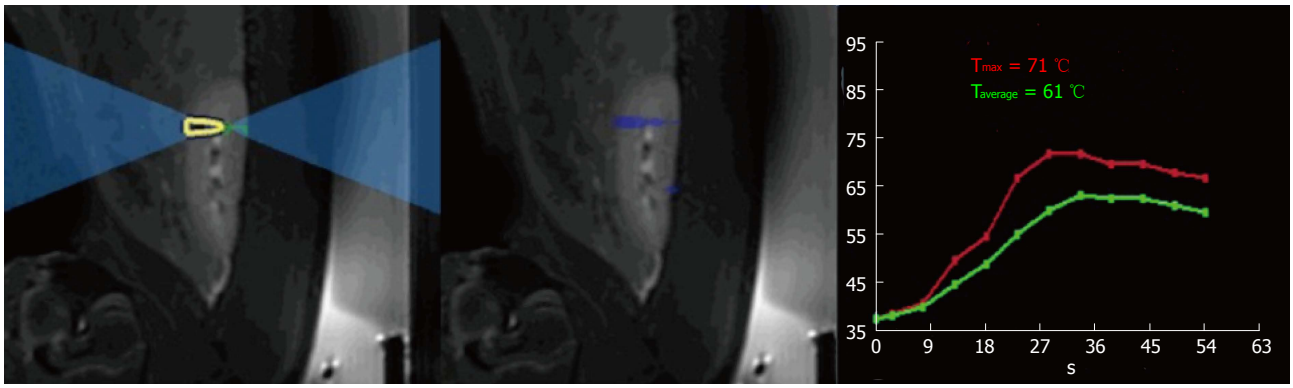

Figure 1 A localizer was performed to verify the position of the kidneys relative to the transducer. Coronal T2-weighted (T2-W) magnetic resonance images show the result of added T2-W treatment planning sequence, which was transferred to the high intensity focused ultrasound software (left and center). The right plot shows the temperature rise during ablation in the renal parenchyma. The red temperature curve represents the maximum temperature measured at the point of focus, while the green curve represents the average temperature in the region of interest.

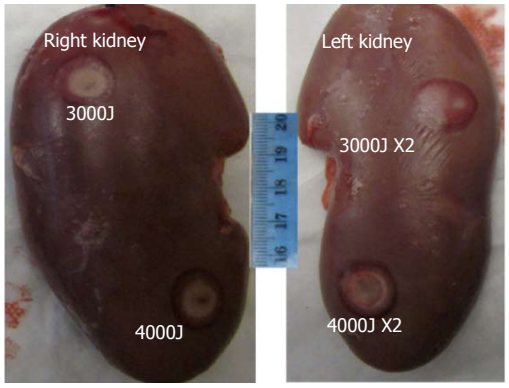

Figure 2 Macroscopic dorsal lesions in the right (single sonication) and left (double sonication) kidney are shown after high intensity focused ultrasound. Note the doughnut-shape hemorrhage (dark red) is surrounding coagulation necrosis (pale). Double sonication at 4400J produced larger lesions compared with the others.

GE, Milwaukee, WI). The back hair was shaved and closely examined for any defects or scars, which might impede the propagation of acoustic energy from the transducer. The pigs were then placed onto the scanner table in a supine position, inside a shallow bath filled with degassed water, so both non-tumor kidneys were centered above the transducer.

Increases in temperature were monitored using phase-differences in fast spoiled gradient-echo sequences (proton resonant frequency shift method) in renal parenchyma. A low-energy test sonication was performed in the para-vertebral muscles to confirm accuracy of the system set-up, calibrate the HIFU beam location and the path of the sound waves. All prescribed targets in the kidneys were 1 cm of the proximal and distal poles based on sagittal plane (Figure 1). A total of 24 lesions (4 per animal and 2 per kidney) were created at 2-3 mm from the renal capsule. The energies used in this study were determined in a pilot study (n = 1 pig), where lower energy (< 2000J) showed no visible renal ablation. The used focal spots were similar in size and geometry. In all animals one single sonication of 3000J at the upper (or proximal) pole of the right kidney and one single sonication of 4400J at the lower (or distal) pole of the right kidney were performed. Double sonication at the respective poles of the left kidney was performed. Unlike single sonication in the right kidney, each target in the left kidney was treated with double overlapping sonication of 3000J lasted for 30 s or 4400J lasted for 40 s (Figure 2). In the double sonication, the second sonication was performed in the exact same location as the first. The frequency was constant (1.1 MHz) in all cases, but the cooling times between sonication were 90 s and 132 s for 3000J and 4400J, respectively. The cooling time was determined by the HIFU software and was sufficient to prevent thermal damage related to heat accumulation in non-targeted tissues. Relatively high energies (3000J to 4400J) and low power (100-110W) were needed to produce visible lesions compared with other soft tissue like in the pancreas (1000J and 500-1350W)[19].

MR imaging and analysis

The default body coil and a 64-channel receiver cardiac coil (GE Healthcare, Waukesha, WI) were used in the current study. Axial, coronal and sagittal planes to the kidney were acquired to verify proper position of the transducer and to plan the ablation treatment. Axial and sagittal T2-W fast spin echo (FSE) (T2-W) sequence with fat saturation was used and the acquired images transferred to the HIFU software. MR thermometry was performed, using 3D segmented-EPI during each sonication with multiphase multi-slice echo planar imaging[20,21].

Post-ablation imaging without contrast was performed 60 min after sonication and with contrast media after 90 min. Table 1 shows the used imaging sequences and their parameters. Two-dimensional T2-W, 2D CE T1-weighted (T1-W) FSE and 3D liver acquisition with volume acquisition (LAVA) images were performed before and after ablation. Signal intensity (SI) ratios (ablated lesion SI/normal parenchyma SI) on T2-W and non-enhanced T1-W images were determined to demonstrate the SI differences prior to contrast media administration. Furthermore, perfusion imaging was conducted during

Table 1 Multiple magnetic resonance imaging sequences used for temperature monitoring, characterization and quantification of ablated kidneys

Pulse sequence	TR (ms)	TE (ms)	ETL	rBW (kHz)	Flip angle (degree)	Slice thickness	Matrix size	NEX	Acquisition time (s)
T2-W thermometry	210	18.3	12	15.63	35	4	256 × 192	1	100
2D T2-W FSE (pre and post ablation)	7300	68	12	15.63	11	4	256 × 192	3	400
Perfusion (post ablation)	3.7	1.5	NA	62.5	9	5	96 × 96	1	120
2D T1-W FSE (pre and post ablation[1])	985	7.2	6	31.25	120	5	192 × 192	1	16
3D LAVA (pre and post ablation[1])	3.9	1.5	NA	62.5	15	5	192 × 192	3	240

[1]Both 2-dimensional T1-weighted fast spin echo and 3-dimentional LAVA images. TR: Repetition time; TE: Echo time; ETL: Echo train length; rBW: Receiver bandwidth; NEX: Number of excitation per step; LAVA: Liver acquisitions with volume acquisition.

bolus injection of 0.2 mmol/kg Gd-DTPA (Bayer, Wayne, NJ). Saturation recovery gradient echo sequence was acquired after ablation to monitor regional perfusion in normal and ablated renal parenchyma. Imaging was performed before and during contrast injection. Regional signal intensity was monitored for 2 min after bolus injection of MR contrast media. Signal intensities were measured in the aortic blood (arterial input function), ablated and normal renal parenchyma.

Post-contrast administration, 2D CE T1-W and 3D LAVA images were repeated. LAVA is based on a 3 dimensional spoiled gradient echo pulse sequence. The 3D volumes (cm^3) of ablated renal parenchyma on only CE MRI (showed best delineation) were determined by multiplying the cranial-caudal, transverse and anterior-posterior lengths of each lesion and presented as means ± standard error of the means. On histopathology, each slice (both faces) was digitally photographed and weighed and the volumes (cm^3) of ablated renal parenchyma were measured using planemetric method.

Histopathology

The skin and tissues adjacent to the kidneys were macroscopically examined after each procedure. More than four hours after sonication the animals were heparinized, terminated and perfused *in situ* with 4% formalin to ensure proper tissue fixation. At postmortem, both kidneys and surrounding organs were macroscopically examined *in situ*. The kidneys were excised, transversely sliced, examined and weighed then fixed in buffered formalin for 48 h to delineate ablated lesions. The lesions were measured using planemetric method. For histopathology the slices from the ablated lesions were embedded in paraffin, sectioned (5 μm) and stained with hematoxylin-eosin (H and E) and examined microscopically.

Statistical analysis

Paired Student's *t*-test was performed to compare lesion volumes after different sonication energies. Regional signal intensity on perfusion imaging and lesion masses were presented as means ± standard error of the mean. Kruskal-Wallis test was used as a non-parametric test to compare the extents of ablated lesions measured on MRI and postmortem. The relationship between MRI *in situ* and postmortem data was assessed using Pearson's correlation coefficient. A *P* value of less than 0.05 was considered statistically significant.

RESULTS

MR imaging-guided HIFU was successfully used to create 24 focal renal lesions in 6 animals (4 per animal and 2 per kidney). The duration of renal planning and sonication was between 50-60 min. The sonication caused no change in average core body temperature, heart rate or O_2 saturation (Table 2). Breath-hold, with the use of muscle relaxant, rocuronium bromide, minimized muscle twitching and diaphragm movement motion during sonication and imaging. During ablation, the temperature rise (58 ℃-63 ℃) in the targeted region was monitored (Figure 1).

MRI characterization and quantification

The ablated lesions were not visible (isointense compared with surrounding renal parenchyma) on fat-suppressed T2-W and non-enhanced T1-W images. SI ratios on T2-W and non-enhanced T1-W images were 1.02 ± 0.02 and 1.03 ± 0.01, respectively, suggesting that there was no evidence of edema four hours after treatment.

On the other hand, perfusion imaging during injection of Gd-DTPA demonstrated hypoperfused ablated lesions as wedged-shaped zones (Figure 3). The changes in SI as a function of time were demonstrated in aortic blood, normal and ablated renal parenchyma. The perfusion deficits persisted for 2 min after contrast administration regardless of the sonication energies. Severe ischemia was observed in ablated lesions (Figure 4). We were unable to monitor the first passage indices (max upslope, max SI and time to the peak) of MR contrast media in the kidneys, because there was a trade-off between temporal resolution, spatial resolution and coverage related to the anatomical locations of the left and right kidneys and the lesions in a single kidney being created far from each other.

Furthermore, 2D CE T1-W FSE and 3D LAVA demonstrated the locations of the lesions in the proximal and distal poles of the kidneys (Figure 5). The locations of lesions on these images matched lesions seen on perfusion

Table 2 Regional, core body temperatures, heart rate and oxygen tension monitored during each sonication

Energy dose (Joules)	Temp (max) (℃)	Temp (avg) (℃)	Core body temp (℃)	HR (bpm)	O_2-saturation (%)
Single 3000	57 ± 3	56 ± 3	38.3 ± 0.6	89 ± 5	99 ± 1
Double 3000	61 ± 4	59 ± 4	38.1 ± 0.5	87 ± 4	99 ± 1
Single 4400	63 ± 6	61 ± 6	38.4 ± 0.4	86 ± 5	99 ± 1
Double 4400	63 ± 4	62 ± 5	38.5 ± 0.3	88 ± 4	99 ± 1

bpm: Beat/min. O_2: Oxygen; HR: Heart rate; Temp: Temperature.

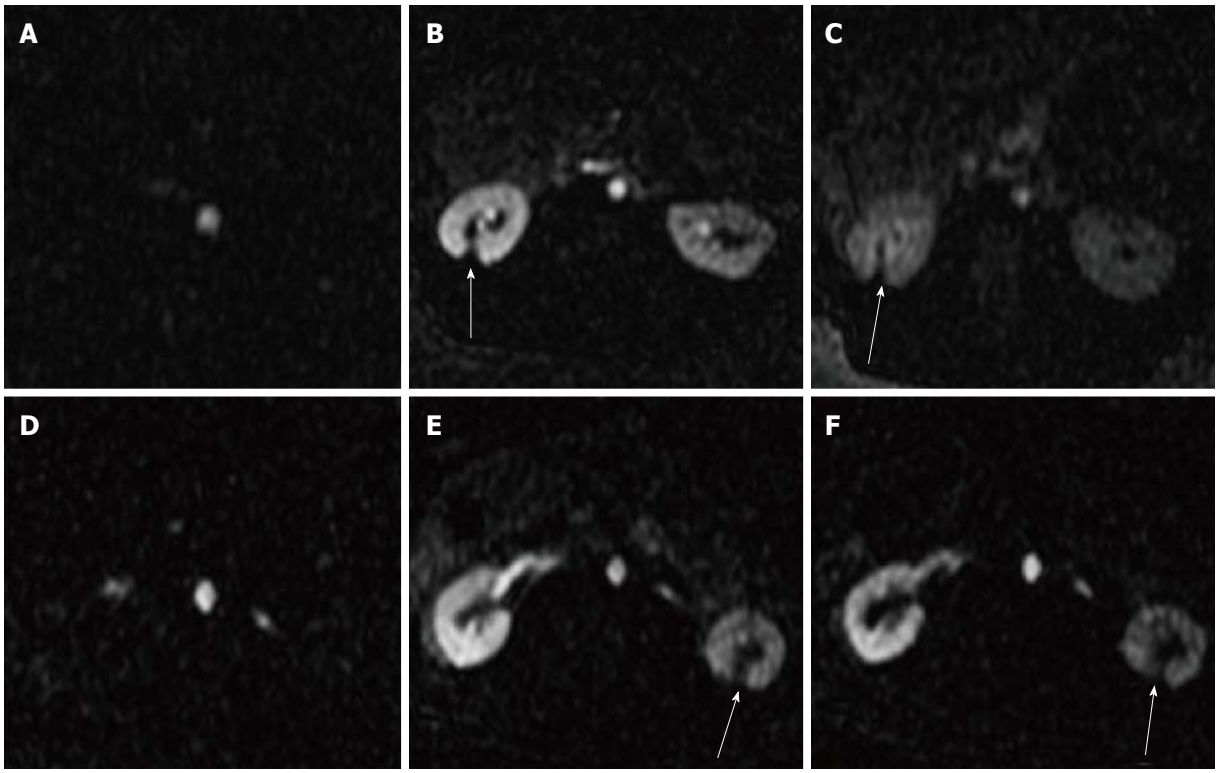

Figure 3 Selected 2D perfusion magnetic resonance images acquired from two representative animals. The images show the arrival of Gd-DTPA bolus (A, D) in the aorta and 20-120 s (B, E and C, F) in the kidneys. Arrows denote the hypoperfused ablated lesions.

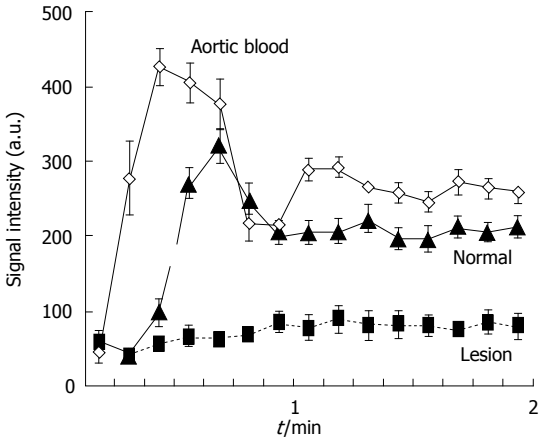

Figure 4 2D magnetic resonance perfusion demonstrates severely hypoperfused ablated lesions after magnetic resonance-guided high intensity focused ultrasound compared to remote non-ablated tissue. Diamond: Aortic blood; Triangle: Viable renal tissue; Square: Ablated lesion. a.u.: Arbitrary units.

MRI. Furthermore, both CE 2D T1-W FSE and 3D LAVA pulse sequences provided good contrast (T1 weighted). On both sequences, a thin hyperenhanced rim was visible around the ablated region on both MRI sequences. Figure 6 shows the wedged-shaped lesions on delayed CE 3D LAVA and 2D T1-W FSE images and macroscopic slices with close correspondence between ablated lesions *in vivo* on MRI and *in vitro* sections.

The average of each lesion dimension and volumes as a function of energy (joules) and sonication number are summarized in Table 3. The lesion volumes within each of the energies varied between animals (0.12-0.36 cm^3 for single sonication 3000J, 0.50-0.84 cm^3 for double 3000J, 0.75-0.784 cm^3 for single 4400J and 0.12-2.65 cm^3 for double 4400J). The ablated volumes on 3000J and 4400J double sonication were significantly larger than single ($P < 0.01$). The ablated volumes on 4400J double sonication were significantly larger than 3000J double sonication ($P < 0.01$).

Table 3 Lesions dimensions and volumes using single and double overlapping rectangular focal sonication

Energy dose (Joules)	CC (mm)	Transverse (mm)	AP (mm)	MRI volume (mm^3)	Postmortem volume (mm^3)
Single 3000	7.3 ± 0.07	7.8 ± 1.0	5.6 ± 0.1	317 ± 54	380 ± 111
Double 3000	7.9 ± 1.1	11.4 ± 1.6	7.5 ± 0.7	675 ± 41[a,c]	587 ± 28[a]
Single 4400	7.5 ± 0.7	7.8 ± 1.6	5.6 ± 0.7	354 ± 143	517 ± 52
Double 4400	11.4 ± 1.7	12.8 ± 3.0	10 ± 1.4	1450 ± 458[a,e,h]	1280 ± 238[a,e,h]

[a]$P < 0.05$ 2 × 3000J overlapping sonication *vs* single 3000J sonication; [c]$P < 0.05$ 2 × 3000J overlapping sonication *vs* single 4400J sonication; [e]$P < 0.05$ 2 × 4000J sonication *vs* single 3000J sonication; and [h]$P < 0.01$ 2 × 4000J overlapping sonication *vs* 2 × 3000J overlapping sonication. CC: Cranial-caudal; AP: Anterio-posterior; MRI: Magnetic resonance imaging.

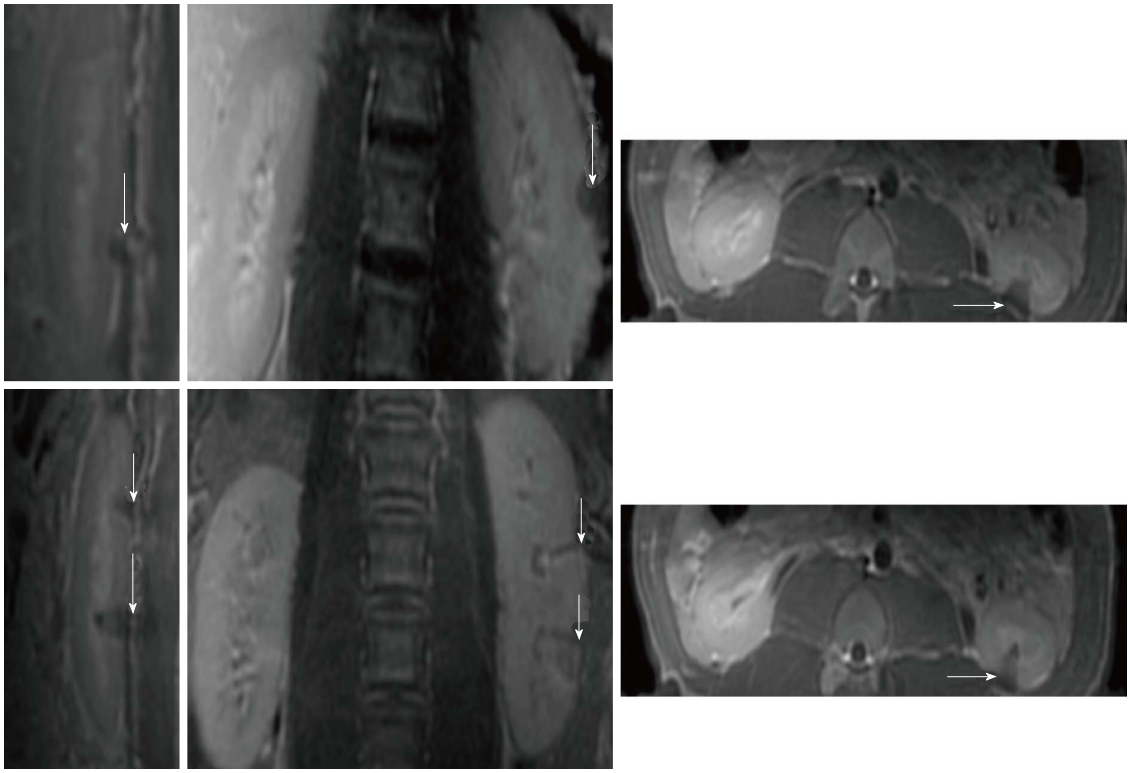

Figure 5 Renal lesions on three magnetic resonance imaging views acquired 3 h after sonication using single 4400J (top row, animal 1) and double 4400J (bottom row, animal 2). The wedge-shape hypoenhanced lesions are seen on contrast enhanced T1-weighted fast spin echo images in sagittal (left images), coronal (center images) and axial (right images) views.

On CE T1-W MRI, the transverse and anterio-posterior dimensions were significantly larger on double sonication (3000J or 4400J) compared with single. Cranial-caudal dimension was significantly larger on double 4400J compared with all other energies and number of sonication. Single sonication of 3000J compared with 4400J produced no significant difference. Paired Student's *t*-test revealed no significant difference in the lesion volumes measured *in situ* on MRI and postmortem (Table 3).

Histopathology characterization and quantification

At postmortem, minor skin burns were observed in two animals and one in the adjacent intestine at double 4400J energy. During postmortem laparotomy no bleeding was found in the peritoneal cavity. In the kidneys, the ablated lesions and surrounding hemorrhage were visible by the naked eye (Figure 2). Renal axial slices showed predominantly wedged-shaped confluent necrotic renal parenchyma (pale) surrounded by hemorrhagic zone (dark red) (Figure 6).

Quantitative analysis of the volumes of ablated parenchyma revealed significant difference between double sonication at 3000J and 4400J and single. Single 3000J and 4400J sonication caused no significant difference in the volumes of ablated parenchyma (Table 3). The data indicate that two overlapping sonication of 4400J are required to produce large lesions > 1.4 cm^3. The lesion volumes within each energies varied between animals (0.23-0.52 cm^3 for single sonication 3000J, 0.25-0.82 cm^3 for double 3000J, 0.45-0.68 cm^3 for single 4400J and 0.29-1.80 cm^3 for double 4400J. Pearson's test showed close correlation between *in situ* MRI and postmortem analysis of ablated parenchyma ($r = 0.98$, $y = -0.19 + 0.13x$, $P < 0.001$) (Figure 7).

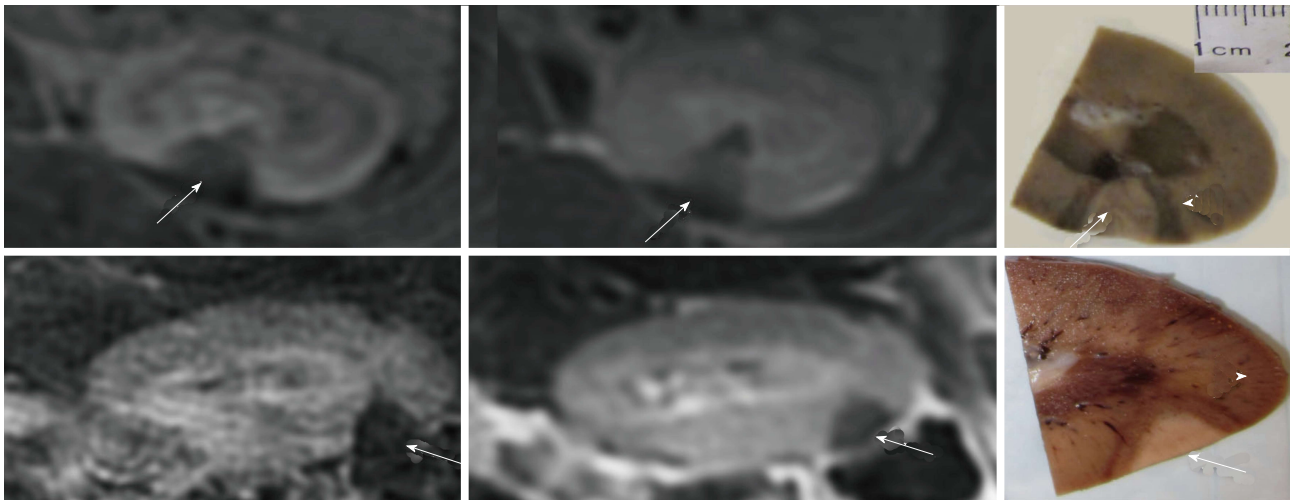

Figure 6 The wedge-shape lesions on contrast enhanced liver acquisitions with volume acquisition (left) and T1-weighted fast spin echo (center) images and gold-standard macroscopic slices (white arrows) from 2 animals (top and bottom rows). Note the close correspondence of ablated lesions *in situ* and *in vitro*. Coagulation necrosis (white arrows) is surrounded by hemorrhagic zone (arrowheads) as shown macroscopically.

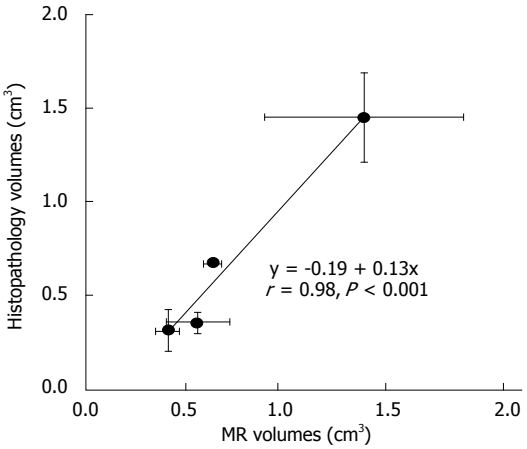

Figure 7 A close correlation was found between *in situ* magnetic resonance imaging and postmortem renal ablation volumes. The bars in the x- and y-axes represent the standard error of the means. The ablated volumes after single sonication at 3000J and 4400J were not significantly different, while volumes at double sonications were significantly larger on both 4400J than 3000J. Furthermore, the effect of double sonications at 4400J was significantly larger than the other energies.

At the cellular level, ablated parenchyma showed necrotic cells in the core of the lesion, hemorrhage at the rim and vascular damage. The necrotic renal parenchyma was without nuclei, opaque and eosinophilic, due to the denaturation of proteins. Intracellular details were lost, which is typical of coagulation necrosis containing outlines of enucleated cells. No evidence of inflammation or peri-renal parenchyma injury was found (Figure 8).

DISCUSSION

The major findings are that (1) noninvasive MRI provided an instant sense of temperature elevation and quantification of renal ablated lesions demonstrated by focal perfusion deficits and necrosis in order to monitor the effects of a range of energies on MRg-HIFU; (2) volumes of renal damage on MRg-HIFU are energy (Joules) dependent; (3) lesion volumes measured *in situ* on MRI and postmortem specimens showed good correlation, despite the difference in the methods of measurement; and (4) macroscopic examination confirmed lesion location and wedged-shape necrosis, while microscopic examination revealed coagulation necrosis, microvascular damage and hemorrhage in the ablated target.

We found that the best contrast between the ablated lesion and normal renal parenchyma is on perfusion, CE 2D T1-W FSE and CE 3D LAVA in a clinically feasible scan time. Although T2-W FSE provides better anatomical information within the kidney, the contrast between the lesion and normal renal parenchyma was poor on T2-W and non-enhanced T1-W images (1.02 ± 0.02 and 1.03 ± 0.01, respectively). The capsules were not visible on T2-W MRI to determine the degree of damage because of the use of fat saturation sequence, but microscopy confirmed the lack of damage in peri-renal renal parenchyma (Figure 8). Wile *et al*[22] found that the ablated lesions become difficult to visualize on fat-suppressed T2-W, since the lesion is isointense relative to surrounding suppressed fat.

MRI and computed tomography (CT) play important roles in guiding renal tumor ablation[22]. However, CE CT was limited in detecting post-ablation (12 mo) lesions. Furthermore, given the need for ionizing radiation on CT, multiple ablation procedures and follow-up imaging, it is likely that MRI will assume an increased role in longitudinal monitoring after renal ablation[23]. The 3T MR-guided system satisfies the requirements of HIFU ablation by providing temperature mapping, high spatial resolution images of target soft tissues and perfusion data. It also provides better features, such as twice the SNR/CNR and uniform fat suppression compared with 1.5T system[24].

This noninvasive study used a 3T MR-guided HIFU and energies (Joules, InSightec) as units of ablation

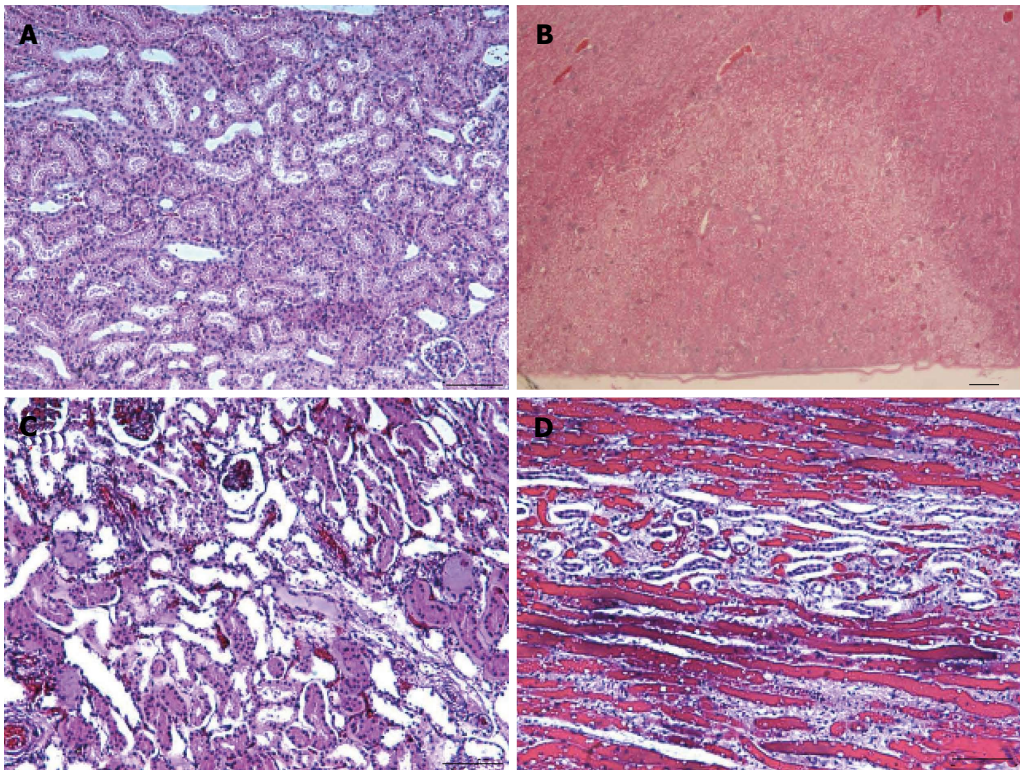

Figure 8 Microscopic sections (hematoxylin-eosin) of a normal renal tissue (A, × 40), the territory of both ablated (pale) and normal renal tissue (B, × 10) and ablated lesion (C, × 40) with damaged nephrons in a haphazard array and hemorrhage (D, × 100). Note the close agreement in the triangular infarct territory on microscopy and microscopy lesions in Figure 6 and magnetic resonance imaging in Figure 6. There was no evidence of peri-renal tissue injury (B).

rather than power (Watts, Philips Systems) used in previous studies[25,26]. Recent experimental studies showed the effectiveness of both power (Watts) and energy (Joules) units in ablating tissues[20,21,25-27]. The relationship between energy dose and lesion depth must be considered[20,21], especially in deep-seated tumors, because this relation depends on the type/density/size of targets and microenvironment factors, such as vascularity/perfusion. Other biologic factors, such as different organs or pathologies with variable structures and perfusions, may dictate the variable with greater utility in generating thermal lesions, thus further comparative studies are necessary.

Our histological study indicated that not only renal parenchyma showed coagulation necrosis but also vessels were severely damaged by HIFU treatment. The damaged vessels with coagulated blood most likely played a critical role in abolishing blood perfusion. Wu *et al*[28] suggested that the cause of perfusion deficits after MR-HIFU ablation is vascular damage, while Shaw *et al*[29] presented an integrated multi-stage mechanism through which HIFU-mediated vascular occlusion could occur.

Study limitations

The main limitations of this feasibility study were: (1) the use of non-tumor kidney model to determine the suitable energies, frequency and duration, which may have different acoustic response from the microenvironment of renal cell carcinoma tissue; (2) the renal motion related to the breathing was not navigated, but minimized by a muscle relaxant and breath holding during sonication. The effects of respiratory motion, boney obstacles and/or shallow angle of focused spots on the variability of ablated volumes and depth cannot be excluded; and (3) the used energy for the kidneys caused minor collateral damage in the skin, subcutaneous muscles and intestine in two animals. Similar cutaneous and subcutaneous tissue burning was previously observed in patients[9].

In conclusion, this MRI and histopathology study provided good assessment of non-tumor renal ablation created by MRg-HIFU. The volume of renal damage is energy and number of sonication dependent on MRg-HIFU. Contrast enhanced MRI is a good tool for visualization and quantification of ablated tissues.

ACKNOWLEDGMENTS

We would like to thank Carol Stillson for her technical support in the experimentation.

COMMENTS

Background

Renal carcinoma constitutes the majority of kidney malignancies. The increased use of high-resolution diagnostic imaging has led to the serendipitous detection of small renal tumors in asymptomatic patients with small masses of renal carcinoma. The gold standard procedure for treatment of localized renal carcinoma remains surgical excision, however, in a large number of patients, surgical excision is precluded by increased perioperative risk due to medical

comorbidities.

Research frontiers

The combination of 3T magnetic resonance imaging (MRI) and MR-guided high intensity focused ultrasound (MRg-HIFU) is suited for noninvasive renal and other tissues ablation. Ablated tissue is well defined on MRI and reflects macro and micro-anatomic changes observed at autopsy and microscopy. Furthermore, the volumes of ablated tissue measured on MRI after MRg-HIFU are energy (Joules) dependent and comparable with autopsy.

Innovations and breakthroughs

Radiofrequency ablation has emerged as a treatment option for renal carcinoma population, with the aim of achieving local oncologic control in a nephron-sparing manner, while avoiding the potential morbidity associated with surgical extirpation and general anesthesia. Innovations in the field of thermal ablation procedures and real-time imaging in the last decade have accelerated the development of non-invasive MRg-HIFU.

Applications

Noninvasive MRg-HIFU with MRI may be utilized for diagnostic and therapeutic purposes in cases of renal masses. It reduces morbidity and health care cost.

Terminology

MRg-HIFU is a new noninvasive technique used for treating tumors. Currently, it is used for treating some cases of uterine fibroids, palliation of bone metastases, brain tumor through the skull, breast cancer, prostate and hepatocellular carcinoma. MRI is another noninvasive imaging technique that has the potential to detect and monitor tumor treatment.

Peer-review

The study is well-performed and the results are interesting.

REFERENCES

1 **Siegel R**, Naishadham D, Jemal A. Cancer statistics, 2013. *CA Cancer J Clin* 2013; **63**: 11-30 [PMID: 23335087 DOI: 10.3322/caac.21166]

2 **Campbell SC**, Novick AC, Belldegrun A, Blute ML, Chow GK, Derweesh IH, Faraday MM, Kaouk JH, Leveillee RJ, Matin SF, Russo P, Uzzo RG. Guideline for management of the clinical T1 renal mass. *J Urol* 2009; **182**: 1271-1279 [PMID: 19683266 DOI: 10.1016/j.juro.2009.07.004]

3 **Ljungberg B**, Cowan NC, Hanbury DC, Hora M, Kuczyk MA, Merseburger AS, Patard JJ, Mulders PF, Sinescu IC. EAU guidelines on renal cell carcinoma: the 2010 update. *Eur Urol* 2010; **58**: 398-406 [PMID: 20633979 DOI: 10.1016/j.eururo.2010.06.032]

4 **Huang WC**, Elkin EB, Levey AS, Jang TL, Russo P. Partial nephrectomy versus radical nephrectomy in patients with small renal tumors--is there a difference in mortality and cardiovascular outcomes? *J Urol* 2009; **181**: 55-61; discussion 61-62 [PMID: 19012918 DOI: 10.1016/j.juro.2008.09.017]

5 **Miller DC**, Schonlau M, Litwin MS, Lai J, Saigal CS; Urologic Diseases in America Project. Renal and cardiovascular morbidity after partial or radical nephrectomy. *Cancer* 2008; **112**: 511-520 [PMID: 18072263 DOI: 10.1002/cncr.23218]

6 **Ritchie RW**, Leslie T, Phillips R, Wu F, Illing R, ter Haar G, Protheroe A, Cranston D. Extracorporeal high intensity focused ultrasound for renal tumours: a 3-year follow-up. *BJU Int* 2010; **106**: 1004-1009 [PMID: 20230379 DOI: 10.1111/j.1464-410X.2010.09289.x]

7 **Hynynen K**, Freund WR, Cline HE, Chung AH, Watkins RD, Vetro JP, Jolesz FA. A clinical, noninvasive, MR imaging-monitored ultrasound surgery method. *Radiographics* 1996; **16**: 185-195 [PMID: 10946699]

8 **Dewey WC**. Arrhenius relationships from the molecule and cell to the clinic. *Int J Hyperthermia* 2009; **25**: 3-20 [PMID: 19219695 DOI: 10.1080/02656730902747919]

9 **Trumm CG**, Stahl R, Clevert DA, Herzog P, Mindjuk I, Kornprobst S, Schwarz C, Hoffmann RT, Reiser MF, Matzko M. Magnetic resonance imaging-guided focused ultrasound treatment of symptomatic uterine fibroids: impact of technology advancement on ablation volumes in 115 patients. *Invest Radiol* 2013; **48**: 359-365 [PMID: 23385396 DOI: 10.1097/RLI.0b013e3182806904]

10 **Voogt MJ**, Trillaud H, Kim YS, Mali WP, Barkhausen J, Bartels LW, Deckers R, Frulio N, Rhim H, Lim HK, Eckey T, Nieminen HJ, Mougenot C, Keserci B, Soini J, Vaara T, Köhler MO, Sokka S, van den Bosch MA. Volumetric feedback ablation of uterine fibroids using magnetic resonance-guided high intensity focused ultrasound therapy. *Eur Radiol* 2012; **22**: 411-417 [PMID: 21901565 DOI: 10.1007/s00330-011-2262-8]

11 **Catane R**, Beck A, Inbar Y, Rabin T, Shabshin N, Hengst S, Pfeffer RM, Hanannel A, Dogadkin O, Liberman B, Kopelman D. MR-guided focused ultrasound surgery (MRgFUS) for the palliation of pain in patients with bone metastases--preliminary clinical experience. *Ann Oncol* 2007; **18**: 163-167 [PMID: 17030549 DOI: 10.1093/annonc/mdl335]

12 **Hynynen K**, McDannold N, Clement G, Jolesz FA, Zadicario E, Killiany R, Moore T, Rosen D. Pre-clinical testing of a phased array ultrasound system for MRI-guided noninvasive surgery of the brain--a primate study. *Eur J Radiol* 2006; **59**: 149-156 [PMID: 16716552 DOI: 10.1016/j.ejrad.2006.04.007]

13 **Zippel DB**, Papa MZ. The use of MR imaging guided focused ultrasound in breast cancer patients; a preliminary phase one study and review. *Breast Cancer* 2005; **12**: 32-38 [PMID: 15657521]

14 **Wu F**, Wang ZB, Zhu H, Chen WZ, Zou JZ, Bai J, Li KQ, Jin CB, Xie FL, Su HB. Extracorporeal high intensity focused ultrasound treatment for patients with breast cancer. *Breast Cancer Res Treat* 2005; **92**: 51-60 [PMID: 15980991 DOI: 10.1007/s10549-004-5778-7]

15 **Napoli A**, Anzidei M, Ciolina F, Marotta E, Cavallo Marincola B, Brachetti G, Di Mare L, Cartocci G, Boni F, Noce V, Bertaccini L, Catalano C. MR-guided high-intensity focused ultrasound: current status of an emerging technology. *Cardiovasc Intervent Radiol* 2013; **36**: 1190-1203 [PMID: 23474917 DOI: 10.1007/s00270-013-0592-4]

16 **Okada A**, Murakami T, Mikami K, Onishi H, Tanigawa N, Marukawa T, Nakamura H. A case of hepatocellular carcinoma treated by MR-guided focused ultrasound ablation with respiratory gating. *Magn Reson Med Sci* 2006; **5**: 167-171 [PMID: 17139143]

17 **Illing RO**, Kennedy JE, Wu F, ter Haar GR, Protheroe AS, Friend PJ, Gleeson FV, Cranston DW, Phillips RR, Middleton MR. The safety and feasibility of extracorporeal high-intensity focused ultrasound (HIFU) for the treatment of liver and kidney tumours in a Western population. *Br J Cancer* 2005; **93**: 890-895 [PMID: 16189519 DOI: 10.1038/sj.bjc.6602803]

18 **Wu F**, Wang ZB, Chen WZ, Bai J, Zhu H, Qiao TY. Preliminary experience using high intensity focused ultrasound for the treatment of patients with advanced stage renal malignancy. *J Urol* 2003; **170**: 2237-2240 [PMID: 14634387]

19 **Sofuni A**, Moriyasu F, Sano T, Itokawa F, Tsuchiya T, Kurihara T, Ishii K, Tsuji S, Ikeuchi N, Tanaka R, Umeda J, Tonozuka R, Honjo M, Mukai S, Fujita M, Itoi T. Safety trial of high-intensity focused ultrasound therapy for pancreatic cancer. *World J Gastroenterol* 2014; **20**: 9570-9577 [PMID: 25071354 DOI: 10.3748/wjg.v20.i28.9570]

20 **Bucknor MD**, Rieke V, Do L, Majumdar S, Link TM, Saeed M. MRI-guided high-intensity focused ultrasound ablation of bone: evaluation of acute findings with MR and CT imaging in a swine model. *J Magn Reson Imaging* 2014; **40**: 1174-1180 [PMID: 24925593 DOI: 10.1002/jmri.24451]

21 **Bucknor MD**, Rieke V, Seo Y, Horvai AE, Hawkins RA, Majumdar S, Link TM, Saeed M. Bone remodeling after MR imaging-guided high-intensity focused ultrasound ablation: evaluation with MR imaging, CT, Na(18)F-PET, and histopathologic examination in a swine model. *Radiology* 2015; **274**: 387-394 [PMID: 25302829 DOI: 10.1148/radiol.14132605]

22 **Wile GE**, Leyendecker JR, Krehbiel KA, Dyer RB, Zagoria RJ. CT and MR imaging after imaging-guided thermal ablation of renal neoplasms. *Radiographics* 2007; **27**: 325-339; discussion 339-340 [PMID: 17374856]
23 **Davenport MS**, Caoili EM, Cohan RH, Ellis JH, Higgins EJ, Willatt J, Fox GA. MRI and CT characteristics of successfully ablated renal masses: Imaging surveillance after radiofrequency ablation. *AJR Am J Roentgenol* 2009; **192**: 1571-1578 [PMID: 19457820 DOI: 10.2214/AJR.08.1303]
24 **Fukatsu H**. 3T MR for clinical use: update. *Magn Reson Med Sci* 2003; **2**: 37-45 [PMID: 16210818]
25 **Wijlemans JW**, de Greef M, Schubert G, Bartels LW, Moonen CT, van den Bosch MA, Ries M. A clinically feasible treatment protocol for magnetic resonance-guided high-intensity focused ultrasound ablation in the liver. *Invest Radiol* 2015; **50**: 24-31 [PMID: 25198833 DOI: 10.1097/RLI.0000000000000091]
26 **Wijlemans JW**, Deckers R, van den Bosch MA, Seinstra BA, van Stralen M, van Diest PJ, Moonen CT, Bartels LW. Evolution of the ablation region after magnetic resonance-guided high-intensity focused ultrasound ablation in a Vx2 tumor model. *Invest Radiol* 2013; **48**: 381-386 [PMID: 23399810 DOI: 10.1097/RLI.0b013e3182820257]
27 **Zibly Z**, Graves CA, Harnof S, Hadani M, Cohen ZR. Sonoablation and application of MRI guided focused ultrasound in a preclinical model. *J Clin Neurosci* 2014; **21**: 1808-1814 [PMID: 25012486 DOI: 10.1016/j.jocn.2014.04.008]
28 **Wu F**, Chen WZ, Bai J, Zou JZ, Wang ZL, Zhu H, Wang ZB. Tumor vessel destruction resulting from high-intensity focused ultrasound in patients with solid malignancies. *Ultrasound Med Biol* 2002; **28**: 535-542 [PMID: 12049967 DOI: 10.1016/S0301-5629(01)00515-4]
29 **Shaw CJ**, ter Haar GR, Rivens IH, Giussani DA, Lees CC. Pathophysiological mechanisms of high-intensity focused ultrasound-mediated vascular occlusion and relevance to non-invasive fetal surgery. *J R Soc Interface* 2014; **11**: 20140029 [PMID: 24671935 DOI: 10.1098/rsif.2014.0029]

P- Reviewer: Stavroulopoulos A **S- Editor**: Gong XM **L- Editor**: A
E- Editor: Lu YJ

Published by **Baishideng Publishing Group Inc**
8226 Regency Drive, Pleasanton, CA 94588, USA
Telephone: +1-925-223-8242
Fax: +1-925-223-8243
E-mail: bpgoffice@wjgnet.com
Help Desk: http://www.wjgnet.com/esps/helpdesk.aspx
http://www.wjgnet.com